Physics in Medicine & Biology

IPEM Institute of Physics and Engineering in Medicine

PAPER • OPEN ACCESS

A wideband model to evaluate the dielectric properties of biological tissues from magnetic resonance acquisitions

To cite this article: Flavia Liporace and Marta Cavagnaro 2024 *Phys. Med. Biol.* **69** 195001

IOP Publishing Phys. Med. Biol. 69 (2024) 195001 https://doi.org/10.1088/1361-6560/ad708b

Physics in Medicine & Biology

IPEM Institute of Physics and Engineering in Medicine

OPEN ACCESS

RECEIVED
11 January 2024

REVISED
29 July 2024

ACCEPTED FOR PUBLICATION
16 August 2024

PUBLISHED
18 September 2024

PAPER

A wideband model to evaluate the dielectric properties of biological tissues from magnetic resonance acquisitions

Flavia Liporace* **and Marta Cavagnaro***

Department of Information Engineering, Electronics and Telecommunications, Sapienza University of Rome, Via Eudossiana 18, Rome 00184, Italy

* Authors to whom any correspondence should be addressed.

E-mail: flavia.liporace@uniroma1.it and marta.cavagnaro@uniroma1.it

Keywords: dielectric properties, magnetic resonance, model, *in vivo*

Abstract

Objective. Aim of this work is to illustrate and experimentally validate a model to evaluate the dielectric properties of biological tissues on a wide frequency band using the magnetic resonance imaging (MRI) technique. *Approach*. The dielectric behaviour of biological tissues depends on frequency, according to the so-called relaxation mechanisms. The adopted model derives the dielectric properties of biological tissues in the frequency range 10 MHz–20 GHz considering the presence of two relaxation mechanisms whose parameters are determined from quantities derived from MRI acquisitions. In particular, the MRI derived quantities are the water content and the dielectric properties of the tissue under study at the frequency of the MR scanner. *Main results.* The model was first theoretically validated on muscle and fat using literature data in the frequency range 10 MHz–20 GHz. Results showed capabilities of reconstructing dielectric properties with errors within 16%. Then the model was applied to ex vivo muscle and liver tissues, comparing the MRI-derived properties with data measured by the open probe technique in the frequency range 10 MHz–3 GHz, showing promising results. *Significance*. The use of medical techniques based on the application of electromagnetic fields (EMFs) is significantly increasing. To provide safe and effective treatments, it is necessary to know how human tissues react to the applied EMF. Since this information is embedded in the dielectric properties of biological tissues, an accurate and precise dielectric characterization is needed. Biological tissues are heterogenous, and their characteristics depend on several factors. Consequently, it is necessary to characterize dielectric properties *in vivo* for each specific patient. While this aim cannot be reached with traditional measurement techniques, through the adopted model these properties can be reconstructed *in vivo* on a wide frequency band from non-invasive MRI acquisitions.

1. Introduction

Nowadays, many medical techniques are based on the application of electromagnetic fields (EMFs) on the human body with diagnostic and/or therapeutic purposes (Mattsson and Simkò 2019). To achieve the best performances and safe and effective results, it is necessary to know the effects generated by the EMF inside the biological system under exposure. To do that, the dielectric properties of the human body must be characterized. Dielectric properties, defined by the complex dielectric permittivity, represent in fact the response of a material to an external applied EMF (Sebek *et al* 2016, Martinsen and Heiskanen 2023). Human and animal tissues are complex and heterogeneous, and their properties can change depending on the subject, the physiological and pathological conditions, and so on (Peyman *et al* 2015). For this reason, the dielectric characterization must be obtained *in vivo* and specifically for each subject of interest. Among the traditional dielectric spectroscopy methods, i.e. adopted for the dielectric characterization of materials, the open-ended coaxial probe is the most used one, mainly because it can give results in a wide frequency band and needs minimal manipulation of the material under test (MUT) (Gregory and Clarke 2007). The experimental set-up of the open-ended coaxial probe is very simple and is constituted of a coaxial cable and a

Vector Network Analyzer (VNA). One of the extremities of the cable is placed in contact with the MUT and the other is connected to the VNA. From the reflection phenomenon that takes place at the interface between the cable's tip and the MUT, and through some mathematical models, it is possible to derive the dielectric properties of the material of interest that, in this work, is represented by biological tissues (Mosig *et al* 1981, Stuchly *et al* 1982, Marsland and Evans 1987). Since there is the need of a direct contact between the cable and the MUT, this technique can be adopted for dielectric spectroscopy of ex vivo biological tissues only. Same considerations can be developed for other traditional techniques, as e.g. the transmission line ones (Stuchly and Stuchly 1980).

In this work, the magnetic resonance imaging (MRI) technique, commonly used for diagnostic purposes, is considered as an alternative method for the derivation of dielectric properties of biological tissues. Recently, different approaches have been proposed to solve this task through MRI acquisitions. One imaging approach starts from the derivation of the water content distribution in the tissues from MRI (Mazzurana *et al* 2003); then the dielectric properties at a certain frequency are associated to this quantity through empirical relations derived using data from the literature (Michel *et al* 2017). This procedure, known as water content electric properties tomography (w-EPT), relies on literature data which typically come from measurements made on ex vivo, mostly animal, biological tissues. Another procedure relates water content and dielectric properties through mixtures theories (Tuncer *et al* 2002). Since mixtures theories are valid at a single frequency, this method—as the previous one—does not give wideband results. In addition to that, mixture theories based on water content are valid at high frequencies only (>1 GHz) and are more accurate for tissues with high water content (>40%) (Farace *et al* 1997, Mazzurana *et al* 2003). A different approach directly relates a parameter of the MRI signal, as e.g. the longitudinal relaxation time (T1), to the corresponding tissue and then assigns to that tissue the dielectric properties reported in public databases (Hasgall *et al* 2022, Andreuccetti *et al* 1997). Using this approach, models of breast (Pelicano *et al* 2021) and of axillary lymph nodes (Godinho *et al* 2021) were developed. In this procedure however, as in the w-EPT method, the properties assigned to a certain tissue are not the ones of the patient but are average values taken from the literature and mostly derived from animal samples. Finally, several research groups are working on the classical (EPT, Liu *et al* 2017, Sadleir and Minhas 2022) approach, which is based on the acquisition of the spatial distribution of the transmit radiofrequency magnetic field B1 in the MUT, i.e. the biological tissues of the patient, for the imaging of the dielectric properties. From the spatial distribution of the B_1 transmit field, the dielectric properties of the tissues are derived at the frequency of the MR scanner using procedures specifically designed for this aim. Among them there are forward methods (Katscher *et al* 2009), inversion techniques (Leijsen *et al* 2021), and deep learning approaches (Mandija *et al* 2019). The level of accuracy and precision of EPT depends on the used MR system, sequences, and related mathematical models. From the different EPT studies, it was found that the maximum reachable accuracy is around 10% using deep learning approaches while simpler methods show higher variabilities (Voigt *et al* 2010, van Lier *et al* 2014, Mandija *et al* 2019). The main limitation of this approach is that it gives results at the single frequency of the MR scanner that, for the most common systems which work at 1.5 T or at 3 T, is 64 MHz or 128 MHz, respectively (Grover *et al* 2015). Accordingly, EPT cannot be useful for medical techniques which apply EMFs at frequencies different from the ones of MR systems. As an example, oncological hyperthermia uses frequencies which go from 70 MHz to 150 MHz for deep tumours and from 434 MHz to 915 MHz for superficial ones (Cihoric *et al* 2015). While 70 MHz is close to 64 MHz, the dielectric properties at 150 MHz cannot be represented by those at 64 MHz. Similarly, dielectric properties at 434 MHz and at 915 MHz are very far from those at 64 MHz or 128 MHz (Grover *et al* 2015).

The aim of this work is to demonstrate and experimentally validate a model for the wideband characterization of the dielectric properties of biological tissues starting from MRI data. The achieved values can be thus useful for different medical techniques applying EMF in a frequency range from 10 MHz to tens of GHz. Indeed, this approach can be applied for the already cited hyperthermia applications (70–150 MHz, 434–915 MHz), for thermal ablation (915 MHz, 2.45 GHz, 5.8 GHz) (Sebek *et al* 2016) and for implanted sensors that work in a wide frequency band (400 MHz–2 GHz) (Malik *et al* 2021). The model is based on the combination of the Cole–Cole dispersion model (Gabriel *et al* 1996) typical of biological tissues and of mixture's theories. The model's parameters rely on the evaluation of the water content of tissues and on the determination of their dielectric properties at the MRI scanner frequency, through the forward EPT approach.

The model has been proposed in previous works (Liporace and Cavagnaro 2023) considering a single high water content tissue and it was theoretically applied with literature data only. In those papers, no analytical explanation was given. In the current work, the derivation of the model is provided in all its steps and the terms present in it are described for the tissues of interest, i.e. those comprehended in the pelvic area of the body. Then the approach is applied theoretically taking the needed data from literature, and a sensitivity analysis, to evaluate the variability in the dielectric properties' values obtained from the model

from the variability of the input quantities, is performed. Finally, the model is applied for the first time on ex vivo muscle and liver tissues using data from MR acquisitions. To have a reference data for the experimental validation, the open-ended probe technique is used to measure the dielectric properties of the available samples.

2. Material and methods

In this section, after a brief introduction on the frequency dependence of dielectric properties, the adopted dielectric model is presented, dividing its structure in a low and a high-frequency contribution. Then, the methods used to validate it are presented, followed by the experimental ones.

2.1. Dielectric behaviour of biological tissues

The dielectric properties of a material are represented by the dielectric permittivity ε and the magnetic permeability μ

$$\varepsilon = \varepsilon_0 \varepsilon_R \tag{1}$$

$$\mu = \mu_0 \mu_R. \tag{2}$$

The dielectric permittivity (equation (1)) represents the reaction of the material to an applied electric field and depends on the dielectric permittivity of vacuum ε_0 (8.854 10–12 F m^{-1}) and on the relative dielectric permittivity of the medium ε_R. The magnetic permeability (equation (2)) corresponds instead to the reaction to an applied magnetic field and is dependent on the magnetic permeability of vacuum μ_0 (1.225666 10–6 H m^{-1}) and on the relative magnetic permeability of the medium μ_R (Collins *et al* 2002).

In the case of biological tissues, the relative magnetic permeability it is usually considered equal to 1 (Sebek *et al* 2016). In this respect, it has to be noted that iron accumulates in hepatocytes, so that liver could present a magnetic permeability different from 1 (Bonkovsky 1991).

With reference to dielectric permittivity (equation (1)), biological tissues are dispersive media, i.e. dipoles and charges that are present in the tissue cannot follow instantaneously the time changes of the applied electric field. Therefore, these materials present a frequency dependent response that is described by the following complex quantity in the frequency domain

$$\varepsilon_R(\omega) = \varepsilon_R'(\omega) - j\,\varepsilon_R''(\omega) \tag{3}$$

where ω (rad s^{-1}) is the angular frequency. The real part $\varepsilon_R{}'$ represents the energy that is stored in the material when an external EMF is applied, while the imaginary part ε_R'' describes the dielectric losses generated in the material and can be related to the equivalent conductivity σ_{eq} as reported in

$$\sigma_{\text{eq}} = \omega \varepsilon_0 \varepsilon_R'' + \sigma_s \tag{4}$$

where a static contribution (σ_s [S m^{-1}]), related to the ability of the material to carry free charges (Sebek *et al* 2016), is present also. To obtain the dielectric characterization of a medium, it is necessary to determine the frequency behaviour of $\varepsilon_R{}'$ and $\varepsilon_R{}''$ (or σ_{eq}).

The frequency behaviour of the dielectric properties of biological tissues is characterized by four main dispersions (α, β, γ and δ) in the frequency range that goes approximately from 10 Hz to 40 GHz (Gabriel *et al* 1996). The α dispersion (from the Hz region until tens of kHz) depends on the counter ions polarization and is followed by the β dispersion (from hundreds of kHz to hundreds of MHz) that is related to the interfacial polarization. The other two dispersions, γ and δ, are dependent on the relaxation of free and bound water, respectively. While the γ dispersion takes place in the GHz region, the δ one is present at lower frequencies but still in the same region. This latter relaxation is commonly neglected because it has a very low effect on the whole spectrum.

Among the many models used to describe the dielectric behaviour of biological tissues with frequency, the Cole–Cole one is the most accurate and commonly adopted (Gabriel *et al* 1996a, 1996b). It describes the complex permittivity of each tissue in the frequency range 10 Hz–40 GHz with four dispersions through the following four poles formula,

$$\varepsilon(\omega) = \varepsilon_\infty + \sum_{i=1}^{n} \frac{\Delta\varepsilon_i}{1 + (j\omega\tau_i)^{1-\alpha_i}} + \frac{\sigma_s}{j\omega\varepsilon_0} \tag{5}$$

where ε_∞ is the permittivity at frequencies much higher than the ones of the last relaxation mechanism, $\Delta\varepsilon_i$ represents the gap in permittivity of the ith relaxation mechanism (i.e. the difference between the

permittivity at frequencies much lower and much higher than the relaxation one), τ_i is the relaxation time of the ith relaxation, α_i represents a widening parameter whose values are included in the range 0–1, and σ_s is the static conductivity.

The parameters in equation (5) depend on each tissue and on each specific dispersion.

In the frequency range of interest of this work (10 MHz–20 GHz), i.e. corresponding to the working frequencies of the main medical techniques already cited in the previous section, the dielectric behaviour of biological tissues is influenced only by the final part of the β dispersion mechanism, and, neglecting δ, by the beginning of the γ one (Liporace and Cavagnaro 2023). The influence of these two dispersions is reflected in the dielectric model described in the following.

2.2. Structure of the dielectric model

The dielectric model adopted in this work was structured in two terms representing the β and γ dispersion mechanisms, respectively. Each term denotes a different frequency range and has different influencing factors. The low frequency term, modelling the behaviour of β dispersion, covers the range from 10 MHz to about 1 GHz and its parameters are typically related to the histology of the tissues (Pethig and Kell 1987). The high frequency term, representing the γ dispersion, covers the range from about 1 GHz to 20 GHz and its parameters are dependent on the water content of the tissues (Kaatze 2011).

In the following, the two terms of the model are explained, and their derivation is presented.

2.2.1. Dielectric model: high frequency term (1 GHz–20 GHz)

The dielectric behaviour of biological tissues at high frequencies, i.e. the γ dispersion, is mainly related to the presence of free water (Kaatze 2011). For this reason, the high frequency term of the dielectric model can be considered dependent on the water content of tissues and can be derived from the acquisitions of this quantity from MRI signals.

The following equation reports the Cole–Cole formula for the complex permittivity considering the single pole associated with the γ dispersion

$$\varepsilon(\omega) = \varepsilon_\infty + \frac{\varepsilon_s - \varepsilon_\infty}{1 + (j\omega\tau)^{1-\alpha}}. \tag{6}$$

In equation (6), the static conductivity, σ_s, was not considered. This quantity, in fact, influences the dielectric behaviour at very low frequencies, while at higher frequencies, like the ones of the γ relaxation, dielectric losses give the main contribution.

The parameters ε_s, ε_∞, α and τ in equation (6) should be determined for each tissue, bringing to a high complexity in the model derivation if many tissues must be characterized. In this work, however, some parameters were assumed to be the same for most of the biological tissues taken into account and others were related to the water content of tissues only. Indeed, through the analysis of the values of the parameters characterizing the γ dispersion for the different biological tissues reported in the literature (Gabriel *et al* 1996, 1996a, 1996b, Andreuccetti *et al* 1997), it was noticed that (i) ε_∞ has the same value for all the high-water content (>50%) tissues (equal to 4), and the same value for all the low water content (<50%) ones (equal to 2.5);
(ii) the dispersion parameter α is equal to 0.1 for all tissues except fat, bone marrow, bone cortical and bone cancellous for which it is 0.2; (iii) the relaxation time τ has values close to the relaxation time of free water (6.366 ps) (Kaatze 2011). Only for the case of bone cancellous and bone cortical the relaxation time (13.263 ps) is much longer than the one of free water. This can be explained by the fact that bone tissue has a low water content, and, for its solid composition, it contains a high quantity of bound water that has a higher relaxation time with respect to free water (Kaatze 2011). So, in the high frequency part of the adopted model the term ε_∞ was fixed at 4 and 2.5 for high (>50%) and low (<50%) water content tissues respectively. The dispersion parameter α was set as 0.1 for all tissues and the relaxation time τ was taken for all tissues as the one of water (6.366 ps) and for bone tissues as the double of it (12.732 ps). The literature data adopted to fix the parameters of the high frequency part of the model were obtained from measurements done on healthy tissues. For this reason, it is not possible to assume the validity of these fixed values for pathological tissues too. However, due to the dependence of the parameters on the water content, they can be assumed to be valid for the case of tumours since tumoral cells are characterized by an increased amount of water with respect to the healthy conditions.

The remaining parameter to be determined in equation (6) is ε_s. In order to do that, mixture's formulas can be used (Tuncer *et al* 2002). These formulas assume that biological tissues are a mixture of water, that is the main component, and cellular structures and organelles which represent solid inclusions. Accordingly, from the knowledge of the water content of a tissue it is possible to derive, with the proper mixture's relation,

its permittivity. Among the many existing mixtures formulas, Fricke's one was used for high water content tissues (Fricke 1924)

$$\varepsilon_s = \varepsilon_w \left(\frac{1-P}{1+(K-1)P}\right)\left(1+\frac{KP\varepsilon_p}{\varepsilon_w(1-P)}\right) \tag{7}$$

with $K = \left[\frac{(1+x)}{x}\right] + \frac{\varepsilon_p}{\varepsilon_w}$.

For low water content tissues instead, the Maxwell's formula was used (Farace *et al* 1997)

$$\varepsilon_s = \varepsilon_w \frac{2\varepsilon_w + \varepsilon_p - 2P\left(\varepsilon_w - \varepsilon_p\right)}{2\varepsilon_w + \varepsilon_p + 2P\left(\varepsilon_w - \varepsilon_p\right)}. \tag{8}$$

In equations (7) and (8) ε_w represents the permittivity of water and ε_p the permittivity of the solid cellular inclusions. The term ε_w is equal to 74 at body temperature (37 °C) and 80 at ambient temperature (25°) in both formulas. The quantity ε_p is equal to 5 in the Fricke's formula (equation (7)) and is equal to 2.5 in the Maxwell's (equation (8)) one. P is the volume fraction of the inclusion and $(1-P)$ the water volume fraction. The factor K in equation (7) depends on the shape of the inclusions, with x equal to 2 for spheres and 1.5 for prolate ellipsoids (Schepps and Foster 1980), and on the permittivity of the inclusions (ε_p).

Following the above, once the water content of a tissue is derived from MRI (Mazzurana *et al* 2003), the high frequency behaviour of the dielectric properties of that tissue can be evaluated.

2.2.2. Dielectric model: low frequency term (10 MHz–1 GHz) and wideband behaviour (10 MHz–20 GHz)

The EPT approach provides the values of permittivity and equivalent conductivity at the MRI scanner frequency, that is about 64 MHz for a 1.5 T scanner and 128 MHz for a 3 T scanner (Liu *et al* 2017). For this reason, the data obtained through EPT can be used to implement the low frequency part of the model. In this work the MRI scanner frequency considered for the theorical validation of the model was chosen as 64 MHz. Instead, for the experimental application of the model the frequency of 128 MHz was considered since a 3 T scanner was used for the MRI acquisitions.

Schepps and Foster (1980) presented, in their work, the results of dielectric measurements of ex vivo biological tissues conducted in the frequency range from 10 MHz to 17 GHz with different techniques. Through an empirical analysis of the low frequency range, the authors found that at frequencies below 0.1 GHz it was possible to represent the permittivity behaviour with a negative power function of frequency. In this way, Schepps and Foster (1980) represented an approximated low frequency behaviour for all the tissues considered in their study without describing the precise behaviour of each single tissue.

Similarly to Schepps and Foster (1980), in this work the rising curve of the β dispersion (from about 1 GHz down to about 10 MHz) was represented by a term containing a negative power function of the frequency. Then, to derive the dielectric properties of each specific tissue, the parameters of this term must be calculated from the EPT data. The following equations report the real and imaginary part of permittivity according to the considered model

$$\varepsilon_R'(\omega) = \frac{a_R}{f^{b_R}} \tag{9}$$

$$\varepsilon_R''(\omega) = \frac{a_I}{f^{b_I}} \tag{10}$$

where f represents the frequency and the parameters a_R, a_I, b_R and b_I depend on the tissue. It is worth noticing here, that having four different parameters in equations (9) and (10) implies that the real and imaginary part follow a different behaviour with frequency. This is justified by the presence of the contribution of the static conductivity (σ_S) within the imaginary part of the relative permittivity.

The low frequency terms (equations (9) and (10)) were added to the high frequency one (equation (6)) obtaining the wideband complex model of permittivity

$$\varepsilon_R(\omega) = \frac{a_R}{f^{b_R}} - j\frac{a_I}{f^{b_I}} + \varepsilon_\infty + \frac{\Delta\varepsilon}{1+(j\omega\tau)^{1-\alpha}}. \tag{11}$$

In order to derive the low frequency parameters, equation (11) was rationalized and after some mathematical manipulations, the expressions for the real (ε_R') and the imaginary (ε_R'') part of the tissues' dielectric properties were obtained

$$\varepsilon_R'(\omega) = \frac{a_R}{f^{b_R}} + \varepsilon_\infty + \frac{\Delta\varepsilon\left[1+\cos\left(\frac{\pi}{2}(1-\alpha)\right)(\omega\tau)^{1-\alpha}\right]}{\left[1+\cos\left(\frac{\pi}{2}(1-\alpha)\right)(\omega\tau)^{1-\alpha}\right]^2 + \sin^2\left(\frac{\pi}{2}(1-\alpha)\right)(\omega\tau)^{2(1-\alpha)}} \tag{12}$$

$$\varepsilon_R''(\omega) = \frac{a_I}{f^{b_I}} + \frac{\Delta\varepsilon \sin\left(\frac{\pi}{2}(1-\alpha)\right)(\omega\tau)^{1-\alpha}}{\left[1+\cos\left(\frac{\pi}{2}(1-\alpha)\right)(\omega\tau)^{1-\alpha}\right]^2 + \sin^2\left(\frac{\pi}{2}(1-\alpha)\right)(\omega\tau)^{2(1-\alpha)}}. \quad (13)$$

Then, in order to find the values of b_R and b_I, the dielectric properties of the tissues of interest were modelled using the data available in the literature (Hasgall *et al* 2022, Andreuccetti *et al* 1997) and were compared with the frequency behaviour represented by equations (12) and (13). Through an interpolation of the data in the low frequency range, the frequency exponent, i.e. the b_R and b_I parameters, were determined for all tissues. In particular, it was found that the parameter b_R can be set to the same value of 0.95 for all tissues, with the exception of fat and bone marrow, that have the lowest water content, for which the value of 1.2 was obtained. The parameter b_I was set in the range 0.85–0.95. In particular, in the cases in which the static conductivity at 64 MHz has high influence on the imaginary part, b_I is 0.95. Instead, for tissues in which the influence of the static conductivity on the imaginary part is medium or low, the value of b_I is set as 0.90 and 0.85, respectively. It is worth noticing here that the references that were considered for the determination of b_R and b_I represent a reliable database of the dielectric properties of biological tissues that was obtained from the collection of many experimental measurements (Hasgall *et al* 2022, Andreuccetti *et al* 1997). Consequently, it constitutes a reasonable source for the evaluation of the models' terms. To find the value of a_R (a_I) from EPT data, equation (12) (equation (13)) was evaluated at the EPT frequency of 64 MHz (or 128 MHz). Given that all other parameters are now set, and EPT gives the permittivity at the considered frequency, a_R (a_I) remains the only unknown in the equation and can be readily evaluated.

2.3. Theorical validation of the model and sensitivity analysis

The dielectric model was validated using literature data considering muscle and fat, as example of a high-water content and low water-content tissue, respectively. To apply the model on biological tissues, water content information and dielectric properties' value at 64 MHz were needed. Typical values of water content of biological tissues are reported in many literature works. However, different works report different water contents for the same tissue. E.g. for muscle, water content was found to be in the range 72%–79% (Schepps and Foster 1980, Pethig and Kell 1987, Mohammed *et al* 2020) and for fat, water content was found to be in the range 5%–20% (Schepps and Foster 1980, Pethig and Kell 1987, Mohammed *et al* 2020). In this paper, for both tissues the water content reported in the same work (Schepps and Foster 1980), and obtained with the same measurement technique, was considered. So, the value of 79% was considered for muscle and of 9% for fat (Schepps and Foster 1980). The values of dielectric properties at 64 MHz were taken from the Gabriel *et al* work (Gabriel *et al* 1996, Andreuccetti *et al* 1997).

In order to validate the results achieved with the proposed approach, they were compared with the reference values reported in Hasgall *et al* (2022) and Andreuccetti *et al* (1997). To this aim, the percentage error between the real and imaginary part of the dielectric properties obtained in this work (ε_R', ε_R'') and the reference ones ($\varepsilon_{R(\text{ref})}'$, $\varepsilon_{R(\text{ref})}'$) was calculated with the following formulas

$$\Delta\varepsilon_R'\% = \frac{\left|\varepsilon_{R(\text{ref})}' - \varepsilon_R'\right|}{\varepsilon_{R(\text{ref})}'} \cdot 100 \quad (14)$$

$$\Delta\varepsilon_R''\% = \frac{\left|\varepsilon_{R(\text{ref})}'' - \varepsilon_R''\right|}{\varepsilon_{R(\text{ref})}''} \cdot 100. \quad (15)$$

Since in the actual case the acquisition of water content and dielectric properties at the MR scanner frequency is always associated with some variabilities, it is necessary to consider how these could affect the results obtained with the adopted dielectric model. Due to the structure of the model, it is expected that the variability related to the water content derivation should affect mostly the high frequency part of the model. In the same way, the variability related to EPT data should affect mostly the low frequencies. The two variability contributions will influence the wideband results. To take into account the effect of these variabilities on results, a sensitivity analysis of the model was conducted. The variability of tissues' water content measured with MRI was shown to be 1% (Fatouros and Marmarou 1999). The variability of EPT-derived permittivity was 10% (Mandija *et al* 2019) and the same was found for EPT-derived equivalent conductivity (Mandija *et al* 2019). Since the water content measurement uncertainty reported above is very low, the sensitivity analysis of the proposed approach was conducted using the literature values. In fact, the water content of a tissue changes depending on the type of animal, on the condition of the tissue and on the adopted measurement technique. Regarding EPT data instead, the measurement uncertainty was considered. The variabilities were inserted in the model determining how the corresponding real and imaginary part change with respect to the case in which a single value for the water content and EPT data were used.

2.4. Samples' preparation

The model, after being theoretically validated, was experimentally applied on ex vivo samples of muscle and liver. Before performing the MRI acquisitions, the dielectric properties of the samples were measured through the open-ended probe technique. Once purchased, the samples were stored in a refrigerator at 4 °C. The day of the experiment, in the morning they were allowed to warm up at ambient temperature and the open-ended probe measurements were performed. Then the samples were taken back in the refrigerator waiting for the availability of the MRI scanner. Both experimental sessions were conducted on the same day and were concluded in a time frame of approximately 7 h. During the whole procedure care was taken to avoid the loss of water from the samples to try to maintain almost the same conditions between the two experimental sessions.

2.5. Experimental application of the model using MRI acquisitions

After the dielectric model was theoretically validated on muscle and fat, it was adopted for the determination of the dielectric properties of ex vivo muscle and liver animal tissues from MRI acquisitions. To this aim a 3 T Philips head-coil MRI scanner was used and the muscle and liver samples were placed in two different plastic beakers with a diameter of 5 cm each. The high frequency term of the model was derived starting from the water content of the tissues while the low frequency one was determined from their dielectric properties obtained, at the frequency of the MRI scanner (128 MHz), through the classical EPT method. In particular, the EPT data was calculated using the forward approach based on the Helmholtz formulation.

2.5.1. Water content derivation from MRI

The water content of a material cannot be derived directly from MRI acquisitions but can be obtained from some parameters of the received signal. Among them the proton density ρ, the transversal relaxation time T_2 and the longitudinal relaxation time T_1 can be cited (Crooks 1985). In this work, the approach based on T_1 was considered. This latter quantity and the water content (wc) are related through the following empirical formula (Fatouros and Marmarou 1999):

$$\frac{1}{\mathrm{wc}} = A + \frac{B}{T_1} \tag{16}$$

where the coefficients A and B can be derived through a calibration for the specific MRI scanner in use. To do so, the T_1 of materials with a known water content must be measured. Different relations, i.e. different coefficients A and B, must be found for materials with high (>60%), medium (60%–40%) and low (<40%) water content (Mazzurana *et al* 2003). Since this work was focused on the derivation of the water content of muscle and liver, i.e. high water content tissues (Schepps and Foster 1980, Pethig and Kell 1987, Fricke 1924), the empirical relation was obtained for high water content materials. For this reason, the calibration was done using two mixtures of distilled water, NaCl and sugar with a corresponding known water content of 100% and 70%. These mixtures were inserted in beakers with a diameter of 3 cm.

The procedure to derive the T_1 consisted in the use of two spoiled gradient echo sequences with the same parameters (TR = 9 ms, TE = 1.4460 ms) but a different flip angle. One signal (S_1) was derived using a low flip angle, i.e. 2°, while the other signal (S_2) was obtained adopting a flip angle of 50°. The ratio between the signal intensity (SI) of S_1 and S_2 was computed obtaining a function weighted in T_1, i.e. whose grey level depends on this quantity only. Considering the formula of the signal obtained from a spoiled gradient echo sequence (Schabel and Parker 2008), the following ratio weighted in T_1 was obtained

$$\mathrm{SI}_{\mathrm{ratio}} = \frac{M_0 \dfrac{\sin\alpha_1 \left(1 - e^{-\frac{\mathrm{TR}}{T_1}}\right) e^{-\frac{\mathrm{TE}}{T_2^*}}}{1 - \cos\alpha_1 e^{-\frac{\mathrm{TR}}{T_1}}}}{M_0 \dfrac{\sin\alpha_2 \left(1 - e^{-\frac{\mathrm{TR}}{T_1}}\right) e^{-\frac{\mathrm{TE}}{T_2^*}}}{1 - \cos\alpha_2 e^{-\frac{\mathrm{TR}}{T_1}}}}. \tag{17}$$

In equation (17) M_0 is the equilibrium magnetization and α_1 and α_2 the low and high flip angles, respectively. The MRI signal was acquired in a 2D transversal section and consequently the T_1 weighted data and the resulting water content were 2D maps too.

In order to calibrate equation (16), the average value of the T_1 weighted map was computed for the mixtures with 100% and 70% of water content and then the coefficients A and B were determined. The water content of the ex vivo samples was obtained as a map, from the T_1 weighted image, and then as a single average value for each tissue.

To evaluate the uncertainty associated with the procedure of the water content derivation, other two mixtures with a known water content (74% and 90%), but different from those used for the calibration, were

used. The water content of these mixtures was determined with the above reported procedure and then the percentage difference between the derived quantity and the true value was computed. This variability was considered as an index of the uncertainty of the water content determination and was used in the adopted dielectric model to evaluate its influence on the results for muscle and liver. In order to do that, first the model was applied considering the average value of water content obtained for each tissue. Then it was applied adopting the water content affected by the variability.

2.5.2. Forward EPT approach

Among the many EPT approaches, the classical forward one was considered in this work. This approach relies on the Helmholtz equation for homogeneous materials considering a relation between the dielectric properties (ε_R' and σ_{eq}) of the biological tissues under MRI exposure and the transmit component of the radiofrequency magnetic field ${B_1}^{tx}$ i.e. the one with an active role during the transmission of the MRI signal (Leijsen *et al* 2021). This component is characterized by a left-hand circular polarization with respect to the static magnetic field B_0 (directed along the z-axis) and can be defined both in the time and in the frequency domain (Leijsen *et al* 2021). For our aims, the transmit field is defined as a scalar complex quantity in the frequency domain and is given by a combination of the components of the radiofrequency field along the x and the y-axis. In EPT literature, it is common to consider for B_0 an orientation along the negative z axis identifying consequently the transmit radiofrequency field with the positive component ${B_1}^{+}$. Instead, if the static magnetic field B_0 is considered directed along the positive z axis, the radiofrequency field involved in the transmission will be indicated by the negative component ${B_1}^{-}$ (Katscher and van den Berg 2017, Hoult 2000). In this work, for generalisation, the transmit field is represented by the term ${B_1}^{tx}$. The Helmholtz formula for homogeneous materials is given by the following expression

$$\frac{\nabla^2 B_1^{tx}}{B_1^{tx}} = -\left(\omega^2 \mu_0 \varepsilon_0 \varepsilon_R' - j\omega\mu_0\sigma_{eq}\right). \tag{18}$$

The assumption of homogeneity of the materials simplifies the formulation of the problem but loses validity in areas where the dielectric properties are not homogeneous, i.e. at the interface between different tissues (Katscher and van den Berg 2017, Leijsen *et al* 2021). From equation (18) the dielectric properties of the tissue under MRI exposure can be obtained (Leijsen *et al* 2021)

$$\varepsilon_R' = -\frac{1}{\omega^2\mu_0\varepsilon_0}\mathrm{Re}\left(\frac{\nabla^2 B_1^{tx}}{B_1^{tx}}\right) \tag{19}$$

$$\sigma_{eq} = \frac{1}{\omega\mu_0}\mathrm{Im}\left(\frac{\nabla^2 B_1^{tx}}{B_1^{tx}}\right). \tag{20}$$

Adopting the polar decomposition of ${B_1}^{tx}$, equation (18) can be written in the following way (Leijsen *et al* 2021)

$$\frac{\nabla^2 |B_1^{tx}|}{|B_1^{tx}|} - |\nabla\varphi^{tx}|^2 + j\left(2\frac{\nabla|B_1^{tx}|}{|B_1^{tx}|}\cdot\nabla\varphi^{tx} + \nabla^2\varphi^{tx}\right) = -\left(\omega^2\mu_0\varepsilon_0\varepsilon_R' - j\omega\mu_0\sigma_{eq}\right) \tag{21}$$

where $|B_1^{tx}|$ represents the amplitude and φ^{tx} the phase of the transmit field. From equation (21), considering the following assumptions for the amplitude and phase of the transmit field (Leijsen *et al* 2021)

$$\frac{\nabla^2 |B_1^{tx}|}{|B_1^{tx}|} \gg \left|\nabla^2\varphi^{tx}\right| \tag{22}$$

$$\nabla^2\varphi^{tx} \gg \frac{2\nabla|B_1^{tx}|\,|\nabla\varphi^{tx}|}{|B_1^{tx}|} \tag{23}$$

it is possible to obtain the permittivity from the amplitude only and the conductivity from the phase only (Leijsen *et al* 2021).

$$\varepsilon_R' = -\frac{1}{\omega^2\mu_0\varepsilon_0}\frac{\nabla^2|B_1^{tx}|}{|B_1^{tx}|} \tag{24}$$

$$\sigma_{eq} = \frac{1}{2\omega\mu_0}\nabla^2\varphi^{tx}. \tag{25}$$

Depending on the aim of the work and on the chosen Helmholtz formula, it is necessary to determine the amplitude and/or the phase map of the transmit field ${B_1}^{tx}$ from the MRI signal using proper sequences and

procedures. The amplitude of B_1^{tx} can be derived in a direct way from the MRI acquisitions while for its phase it is necessary to consider additional steps. In fact, the measurable phase, called transceive phase, is given by a superposition of the phase contributions of the transmit (B_1^{tx}) and the receive (B_1^{rx}) fields (Leijsen *et al* 2021). However, for low intensities of the static field (1.5 T or 3 T) it is possible to consider that, under the transceive phase assumption, the contributions given by the transmit and the receive phase are the same (Leijsen *et al* 2021). Consequently, it is possible to obtain the transmit phase as half of the measured transceive one.

In this work the simplified Helmholtz approach (equations (24) and (25)) was considered for the determination of the dielectric properties of muscle and liver ex vivo tissues. For the derivation of the amplitude and phase of the transmit field, different MR sequences were adopted obtaining maps with different resolution and dimensions. The amplitude of the transmit field was acquired through the actual flip angle procedure (Yarnykh 2007) based on the use of two spoiled gradient echo sequences with the same parameters (flip angle = 65°, Echo Time TE = 2.3460 ms) but a different repetition time TR (TR_1 = 250 ms, TR_2 = 50 ms). For the acquisition of the transceive phase instead, two Spin Echo sequences (van Lier *et al* 2014) were acquired using the same parameters (flip angle = 90°, TE = 5.16 ms, TR = 900 ms) but gradient of opposite polarities. The transmit phase contribution was obtained as explained above.

The forward Helmholtz method (H-EPT) is simple to implement and, with respect to other EPT approaches like the w-EPT one, is based on formulas with a physical validity. However, it is affected by two main issues. The first one, due to the homogeneity assumption, is associated with boundary effects. The second one is due to the presence of the second order derivative in the formulas (equations (24) and (25)) which results in an amplification of the noise that is present in the field maps. Consequently, when the forward Helmholtz method is used, it is necessary to take into account these issues adopting some procedures for their reduction.

In this work the simplified Helmholtz formulas (equations (24) and (25)) were implemented in MATLAB (ver. R2020b) where the input quantities, i.e. acquired amplitude and phase maps, were loaded as DICOM data. In order to reduce the noise, a Gaussian denoising filter was applied to both amplitude and phase maps. Additionally, a segmentation procedure was applied to isolate the object of interest from the noisy background. Then the Helmholtz formulas were applied deriving the dielectric properties' maps. As last step, the dielectric properties were retained only in those pixels belonging to the tissues in which the derived values were included in a realistic range. In particular, the dielectric properties values should be at minimum equal to the value derived at high frequency (the lower the frequency the higher the dielectric properties) and at maximum equal to the value of saline solution with a 0.9% NaCl concentration (the dielectric properties of water represent an upper limit for the dielectric properties of biological tissue (Andreuccetti *et al* 1997)). Due to the unavoidable noise, an irregular distribution of the retained data was obtained. For this reason, the modal value was determined and considered as representative value of the dataset. The modal represents the value that is present with the highest frequency in the dataset and, for this reason, well describes irregular distributions of data. The standard deviation was also computed for the values higher and lower with respect to the modal value.

As previously reported, the used MRI scanner was a 3 T one. Accordingly, the dielectric properties derived with the Helmholtz EPT approach represent values at the frequency of 128 MHz. They were then used in the model to determine its low frequency term.

2.6. Open-ended probe technique

For validating the results obtained with the dielectric model starting from MRI data, the dielectric properties of the used ex vivo muscle and liver sample tissues were measured in the frequency range 10 MHz–3 GHz with the open probe technique. Measurements were performed prior to put the samples in the MRI scanner. A custom-made set-up, in which the open-ended probe was constituted by a SM250 cable from HUBER + SUHNER AG (Herisau, Switzerland), was adopted. The maximum frequency was fixed at 3 GHz since the measurement sensitivity of the considered cable decreases at frequencies higher than this value (Liporace and Cavagnaro 2022). To reconstruct the dielectric properties of the MUT from the measured reflection coefficients, the Stuchly model was used (Gregory and Clarke 2007). This model requires the measurement of three materials with known dielectric properties (calibration procedure) prior of measuring the MUT. The choice of these terminations depends on the type of MUT. The more the dielectric properties of the terminations are close to those of the MUT, the more accurate the reconstruction obtained with the model will be. For the case of interest, i.e. MUT represented by muscle and liver tissues, the calibration was done using a short circuit (SC), an open circuit (OC) and distilled water (DW). The short circuit was realized with an aluminium sheet while the open circuit was obtained leaving the probe in air.

In order to assess the accuracy of the results, the measurement uncertainty (u) was computed. This quantity is given by the contribution of the measurement accuracy and the measurement repeatability (Taylor and Kuyatt 1994).

In general, the measurement accuracy represents the distance between the measured data and the true ones. In the case of the open-ended probe technique, it must be determined measuring the dielectric properties of a known liquid and comparing them with a reference. In this work, a saline solution with 0.9% NaCl was used as reference liquid (Peyman *et al* 2007), and the percentage error ($\Delta\varepsilon_R'^{(\prime)}\%$) between the measured dielectric properties ($\varepsilon_{R,\,\text{measured}}'^{(\prime)}$) and the reference ones ($\varepsilon_{R,\,\text{reference}}'^{(\prime)}$) was evaluated with the equation

$$\Delta\varepsilon_R'^{(\prime)}\% = \frac{\left|\varepsilon_{R,\,\text{reference}}'^{(\prime)} - \varepsilon_{R,\,\text{measured}}'^{(\prime)}\right|}{\varepsilon_{R,\,\text{reference}}'^{(\prime)}} \cdot 100 \tag{26}$$

where the superscript $'$ and $''$ evidence that the uncertainty is evaluated separately for the real (ε_R') and immaginary (ε_R'') part of the relative permittivity. Then the uncertainty component due to the measurement accuracy (u_{accuracy}) can be calculated considering a rectangular distribution (Taylor and Kuyatt 1994)

$$u_{\text{accuracy},\varepsilon_R'^{(\prime)}} = \frac{\Delta\varepsilon_R'^{(\prime)}}{\sqrt{3}}. \tag{27}$$

The measurement repeatability represents the variation of the results between repeated measurements. It can be evaluated from the percentage standard deviation (sd%) obtained from n measurements:

$$\text{sd}\% = \sqrt{\frac{\sum_{i=1}^{n}(x_i - \bar{x})^2}{n(n-1)}} \cdot 100 \tag{28}$$

where x_i is the ith measurement, $\bar{x}$ is the average of the repeated measurements and n is the number of repetitions. Then the uncertainty associated with the measurement repeatability ($u_{\text{repeatibility}}$) can be derived from equation (28) considering a normal distribution (Taylor and Kuyatt 1994)

$$u_{\text{repeatibility},R,I} = \frac{\text{sd}}{1}. \tag{29}$$

In this work $u_{\text{repeatibility}}$ (equation (29)) was evaluated cutting both muscle and liver tissues into four samples and repeating the measurements five times on each sample, placing the probe's tip in different positions.

The measurement uncertainty was then derived from the combination of the two contributions.

$$u_{R,I} = \sqrt{\left(u_{\text{accuracy},R,I}\right)^2 + \left(u_{\text{repeatability},R,I}\right)^2}. \tag{30}$$

3. Results and discussion

In the following, the high frequency term of the dielectric model is analysed first, showing how the introduced approximations (i.e. to fix the values of some parameters of the formulas) affect the results. Then the dielectric properties of muscle and fat are presented in the frequency range 10 MHz–20 GHz using literature data for the theorical validation of the model. For both tissues, the sensitivity analysis was considered both for the water content and for the EPT data. Finally, the results obtained applying the wideband model on MRI acquisitions are presented for ex vivo muscle and liver tissues in the frequency range 10 MHz–3 GHz.

3.1. Dielectric model: high frequency term

Figures 1 and 2 report, respectively, the real and the imaginary part of permittivity obtained with the Cole–Cole model used as a reference (equation (5)), considering only the pole corresponding to the γ dispersion (Andreuccetti *et al* 1997), and the ones obtained using the same formula with the parameter α fixed to the value of 0.1. The tissues that were taken into consideration are fat, bone marrow, bone cancellous and bone cortical, i.e. all those tissues which are characterized by an α value of 0.2 (Andreuccetti *et al* 1997) that is different from the one used in the approximation.

From the figures it is evident that the approximation considered in this work for the α term did not change in a significant way the high frequency behaviour of dielectric properties with respect to the case in

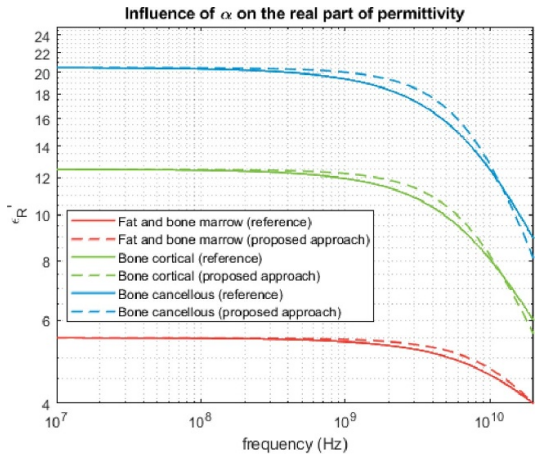

Figure 1. Real part of permittivity.

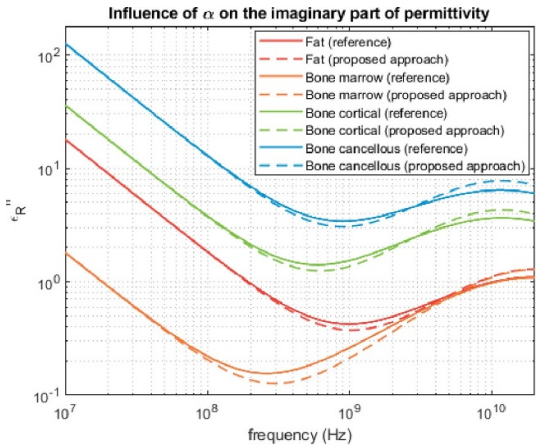

Figure 2. Imaginary part of permittivity.

which the actual value of α was adopted for each tissue. For the real part of permittivity, the percentage error between the data obtained with the actual and the approximated α value was always lower than 10%. For the imaginary part of permittivity, the percentage error was higher, but it is still under 20%.

As a successive step, the relaxation time approximation was considered. In the model, instead of using the specific value of this parameter for each tissue, the one of free water (6.366 ps (Kaatze 2011)) was considered for all tissues but for bone, for which twice the value of free water was used. Tables 1 and 2 show, for the tissues of interest, the maximum value of the relative percentage error obtained between the one pole Cole–Cole reference model, which uses the specific values of α and τ for each tissue, and the one pole Cole–Cole model which uses α equal to 0.1, and the value of τ of free water for all tissues (table 1) and its double for bone tissues (table 2). All other values of the model are the same of the Cole–Cole one (Hasgall *et al* 2022). The percentage error was calculated in the whole frequency range (10 MHz–20 GHz) and the maximum value and the corresponding frequency are reported in the tables. For each tissue the water content is presented too, as derived from literature works (Schepps and Foster 1980, Pethig and Kell 1987, Mohammed *et al* 2020) as well as the τ value and the dispersion parameter of each tissue, reporting the percentage error between them and the values chosen for these parameters in the model.

From the data reported in the tables, it is possible to conclude that, for the real part of permittivity, the maximum error is obtained at 20 GHz for high water content tissues and at lower frequencies for low water content tissues. The imaginary part shows higher differences than the ones obtained for the real part. Maximum errors were found at frequencies between 1 and 5 GHz, with the exception of bone cancellous and bone cortical. As expected, the errors in dielectric properties are higher for those tissues whose relaxation time is more distant from the one of free water. Tissues like muscle, whose relaxation time (7.234 ps) is closer to the one chosen by the adopted model (6.366 ps), show the lowest errors both for the real (7.9%) and the imaginary (8.68%) part of permittivity. On the contrary, tissues like liver, whose relaxation time (8.842 ps) is

Table 1. Percentage error between the Cole–Cole model (Hasgall *et al* 2022) and the adopted high frequency dielectric model, obtained using the approximations for α (constant value of 0.1) and τ (constant value of 6.366 ps). The water content of the tissue is reported also.

Tissue	τ of the tissue (ps)	$\Delta\tau$ (%)	α of the tissue	$\Delta\alpha$ (%)	Maximum error in the frequency range (%)		Water content (%)
					$\Delta\varepsilon_R'$	$\Delta\varepsilon_R''$	
Muscle	7.234	13.7	0.1	0	7.9 (20 GHz)	8.68 (3.8 GHz)	72–79
Cervix	7.958	25	0.1	0	14.6 (20 GHz)	13.8 (4.2 GHz)	76–80
Colon	7.958	25	0.1	0	14.8 (20 GHz)	17 (1.5 GHz)	70–80
Blood	8.377	31.7	0.1	0	19 (20 GHz)	19.2 (5 GHz)	78–80
Small intestine	7.958	25	0.1	0	14.8 (20 GHz)	13.11 (4.6 GHz)	75
Spleen	7.958	25	0.1	0	14.7 (20 GHz)	16.44 (2 GHz)	76–81
Liver	8.842	39	0.1	0	22.5 (20 GHz)	23 (2 GHz)	73–77
Kidney	7.958	25	0.1	0	14.7 (20 GHz)	16 (2.5 GHz)	74–79
Stomach	7.958	25	0.1	0	15.16 (20 GHz)	13.44 (4.4 GHz)	72–78
Uterus	7.958	25	0.1	0	15 (20 GHz)	14.7 (3.5 GHz)	76–80
Bladder	8.842	39	0.1	0	20.6 (20 GHz)	18 (4.7 GHz)	70–80
Bone marrow	7.958	25	0.2	50	7.19 (13 GHz)	32.7 (0.7 GHz)	8–16
Fat	7.958	25	0.2	50	7.19 (13.3 GHz)	22.5 (1.7 GHz)	5–20

Table 2. Percentage error between the Cole–Cole model (Hasgall *et al* 2022) and the adopted high frequency dielectric model, obtained using the approximations for α (constant value of 0.1) and τ (constant value of 12.732 ps) in the case of bone tissues. The water content of the tissue is reported also.

Tissue	τ of the tissue (ps)	$\Delta\tau$(%)	α of the tissue	$\Delta\alpha$(%)	Maximum error in the frequency range (%)		Water content (%)
					$\Delta\varepsilon_R'$	$\Delta\varepsilon_R''$	
Bone (cancellous)	13.263	4.2	0.2	50	8.11 (5.2 GHz)	21.33 (13.6 GHz)	44–55
Bone (cortical)	13.263	4.2	0.2	50	6.17 (5.1 GHz)	17.5 (13.8 GHz)	16–20

Table 3. Model's parameters for muscle and fat.

Tissues	a_R	b_R	a_I	b_I	ε_s	ε_∞	α	τ (ps)
Muscle	1.268	0.95	16.3	0.9	54.9	4	0.1	6.366
Fat	0.036	1.2	0.8329	0.9	5.5	2.5	0.1	6.366

far from the chosen one (about 40% difference), show higher errors, namely around 22.5% for the real part and around 23% for the imaginary one.

3.2. Wideband dielectric properties of muscle and fat: theorical validation of the model

Muscle is a high-water content tissue and for this reason the term ε_∞ was set at 4 and the term ε_s was calculated using the Fricke's mixtures formula, obtaining—for a water content of 79%—a value of 54.9 (equation (7)). Fat is instead a low-water content tissue for which the parameter ε_∞ was set at 2.5, and the Maxwell's mixtures formula was used to obtain ε_s, finding a value of 5.5 (equation (8)) for a water content of 9%. In both cases the relaxation time τ was taken as the one of free water (6.366 ps) and α as 0.1. With reference to the frequency dependence of the low frequency term, exponents of 0.95 and 0.90 were set for the real and imaginary part of muscle, while 1.2 and 0.90 were used for fat, as previously explained. To obtain the wideband dielectric behaviour (equations (12) and (13)) the corresponding values for the parameters characterizing the low frequency contribution of the model were derived using values of the dielectric properties at 64 MHz taken from the literature (Andreuccetti *et al* 1997). In particular, for muscle, the relative permittivity and the conductivity at 64 MHz are 72.235 and 0.68 S m^{-1} respectively (Andreuccetti *et al* 1997). For fat, the values of 6.5064 and 0.035 S m^{-1} were found for relative permittivity and conductivity, respectively (Andreuccetti *et al* 1997). All parameters are reported in table 3.

The parameters reported in the table above were used to obtain the frequency behaviour of the real (figure 3(a)) and the imaginary (figure 4(a)) part of the permittivity of muscle. The results obtained with the high frequency term of the dielectric model are shown with the dashed—dotted blue curve, the ones obtained with the wideband dielectric model with the dashed green curve while the ones obtained from reference data with the continuous red curve. The percentage error between the adopted model and the

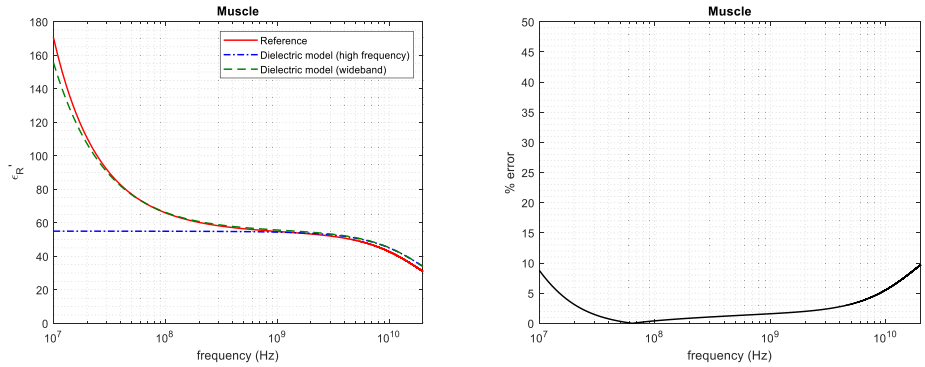

Figure 3. (a) Real part of permittivity of muscle. Red curve: reference values (Hasgall *et al* 2022); dashed—dotted blue curve: high frequency contribution of the dielectric model; dashed green curve: complete dielectric model. (b) Percentage error between the adopted model and the Cole–Cole one (Hasgall *et al* 2022).

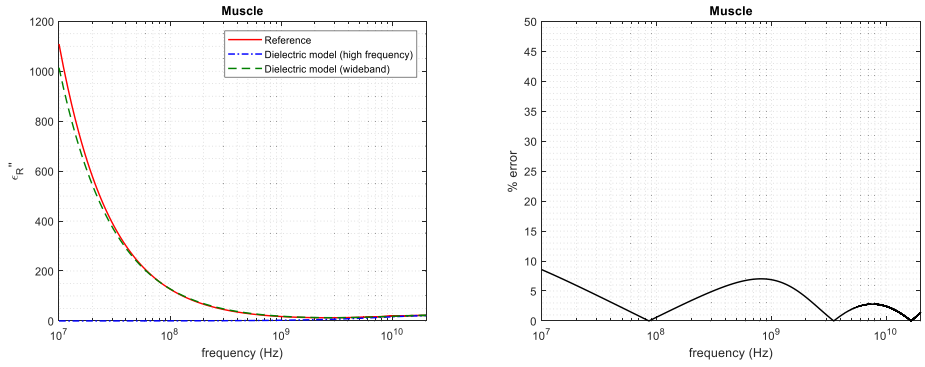

Figure 4. (a) Imaginary part of permittivity of muscle. Red curve: reference values (Hasgall *et al* 2022); dashed—dotted blue curve: high frequency contribution of the dielectric model; dashed green curve: complete dielectric model. (b) Percentage error between the adopted model and the Cole–Cole one (Hasgall *et al* 2022).

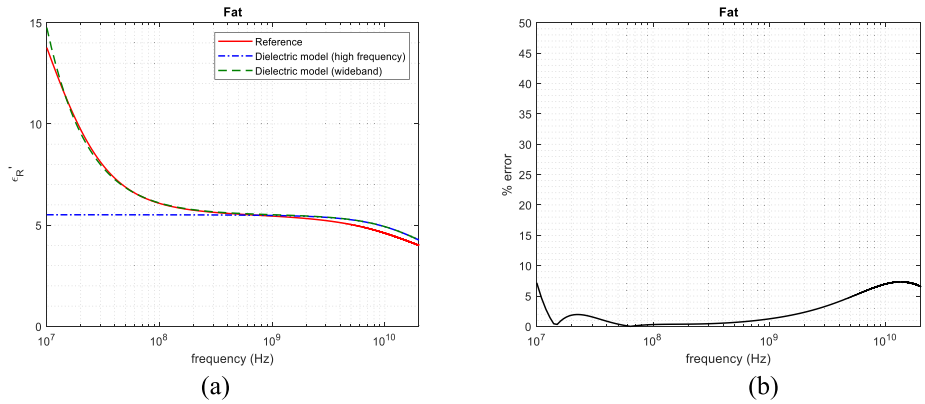

Figure 5. (a) Real part of permittivity of fat. Red curve: reference values (Hasgall *et al* 2022); dashed—dotted blue curve: high frequency contribution of the dielectric model; dashed green curve: complete dielectric model. (b) Percentage error between the adopted model and the Cole–Cole one (Hasgall *et al* 2022).

reference from literature (Andreuccetti *et al* 1997) was computed and is represented in panels (b) of the figures (figures 3(b) and 4(b)).

The same results were obtained for fat using the parameters reported in table 3. The real and the imaginary part of permittivity are reported in figures 5(a) and 6(a) respectively. Figures 5(b) and 6(b) represent the percentage error between the results obtained with the dielectric model and the reference.

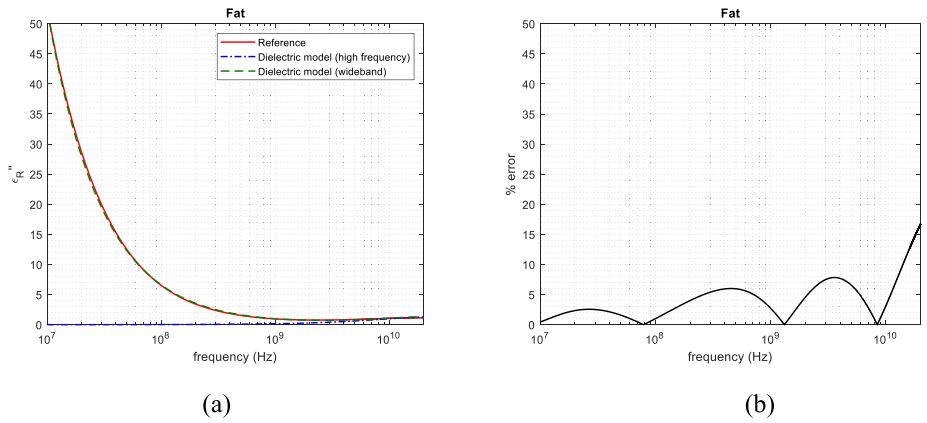

Figure 6. (a) Imaginary part of permittivity of fat. Red curve: reference values (Hasgall *et al* 2022); dashed—dotted blue curve: high frequency contribution of the dielectric model; dashed green curve: complete dielectric model. (b) Percentage error between the adopted model and the Cole–Cole one (Hasgall *et al* 2022).

From the figures it is possible to notice that the results achieved with the model accurately follow the reference values for both tissues. In the case of muscle, the percentage difference is always lower than 10% both for the real (figure 3(b)) and for the imaginary part (figure 4(b)). For the case of fat, the percentage difference is lower than 10% in the whole frequency range for the real part (figure 5(b)) and up to 14 GHz for the imaginary part (figure 6(b)). This can be explained by the fact that the high frequency approximation for the relaxation time gives more accurate results for high water content tissues. It is worth noticing here that the percentage difference reaches its minimum around the frequency of 64 MHz since at this frequency the EPT permittivity value used in the model was the same of the reference one (Hasgall *et al* 2022).

3.3. Sensitivity analysis

In this section, the influence of water content and EPT data on the results achieved with the dielectric model was studied separately first; then, the impact of the combination of the variability of these two quantities was analysed.

As already explained, according to the literature, water content has been derived from MRI with an uncertainty of 1% (Fatouros and Marmarou 1999). Such a low variability has, of course, little influence on the results achieved with the model. In the literature however, different values of water content for the same tissue are reported in different works (72%–79% for muscle and 5%–20% for fat (Schepps and Foster 1980, Pethig and Kell 1987, Mohammed *et al* 2020)), since this quantity depends on tissue conditions and on the used measurement technique. So, the sensitivity analysis with respect to water content was done considering the literature range and not the measurement uncertainty. The sensitivity analysis was conducted also for the measurement uncertainty associated to the EPT data. In this case, a minimum obtainable variability of 10% was reported (Mandija *et al* 2019).

Since in the real case both EPT data and water content quantities are needed and can be affected by variability, it is necessary to determine their combined effect. In order to do that, the percentage difference was calculated between the results found with single-value water content and EPT data and the ones obtained with the combination of the variabilities of both quantities. The combined variabilities of water content and EPT were considered in the worst situation, which corresponds to the case in which both quantities have the maximum deviation from the reference data.

In table 4 the percentage differences in the real and the imaginary part of permittivity at the considered frequencies are reported for muscle. For each frequency, the values obtained for the variability of water content only, for the variability of EPT data only and for the combined variabilities of water content and EPT data are reported.

From table 4 it is possible to notice that, as expected, the difference obtained with only the water content variability increases with frequency. In addition to that, the effect is higher on the real part than on the imaginary one. The difference obtained with the EPT data variability increases instead for decreasing frequencies. In this case the percentage difference is higher for the imaginary part. When the two variability contributions are combined, the obtained percentage difference is higher than the one obtained for the single variabilities and increases for decreasing frequencies due to the stronger influence of EPT variability. Any case, at the frequencies of interest for medical applications, the variation of the model results is below 13%.

Table 4. Results variations for variability of water content (wc) and EPT data for muscle.

	Percentage variability					
	$\Delta\varepsilon_R'(\%)$			$\Delta\varepsilon_R''$ (%)		
Frequency	wc	EPT	wc and EPT	wc	EPT	wc and EPT
70 MHz	0.7	9.36	10.06	0.02	10	10.02
150 MHz	5.4	5.13	10.53	0.05	9.95	10
434 MHz	9.2	2	11.2	0.4	9.64	10.04
915 MHz	10.3	1.03	11.33	1.5	8.75	10.25
2.45 GHz	10.9	0.42	11.32	5.6	5.49	11.09
5.8 GHz	11.2	0.19	11.39	10	2.2	12.2

Table 5. Results variations for variability of water content (wc) and EPT data for fat.

	Percentage variability					
	$\Delta\varepsilon_R'$ (%)			$\Delta\varepsilon_R''(\%)$		
Frequency	wc	EPT	wc and EPT	wc	EPT	wc and EPT
70 MHz	10	9.12	19.12	0.05	10	10.05
150 MHz	46.6	4	50.6	1.08	9.9	10.98
434 MHz	58.7	1.16	59.86	8.2	9.5	17.7
915 MHz	61.6	0.48	62.08	25	8.5	33.5
2.45 GHz	61.8	0.159	61.9	59.3	5.4	64.7
5.8 GHz	61.9	0.058	61.9	75.7	2.14	77.54

As done for the muscle case, the fat water content variability reported in literature works was considered for the sensitivity analysis. In order to do that, the dielectric properties were reconstructed with the model using the minimum (5%) and the maximum (20%) water content values (Schepps and Foster 1980, Pethig and Kell 1987, Mohammed *et al* 2020). The sensitivity to EPT data variability was obtained considering the uncertainty reported in literature (10%) (Mandija *et al* 2019).

In table 5 the percentage difference in the real and the imaginary part of permittivity at the considered frequencies are reported for fat tissue considering the variability of water content (wc) only, the variability of EPT data only, and the two variabilities together.

The same comments reported for muscle can be reported for the fat case also: the influence of water content variability increases with increasing frequency while the one of EPT data increases for decreasing frequencies. However, for the fat tissue, the percentage error due to the water content variability is higher than the one obtained for muscle, bringing also to a higher influence in the combined variability. This different behaviour is obtained because, in the case of fat, the water content variation in the literature was of the 75%, while in the case of muscle is of the 8.8%. Accordingly, for the muscle case, a variation of 8.8% of water content brought to a maximum variation of the results equal to 11.2%, while for the fat case a water content variation of 75% gave a maximum variation in the results equal to 75.7%. In addition to that, the values of dielectric properties of fat are very low and the percentage error computed on them is consequently very high.

From this analysis it is worth concluding that the water content of the tissue should be determined with the highest precision possible, in particular in the low-water content tissues.

3.4. Wideband dielectric properties of ex vivo tissues: experimental validation of the model

In this section the results obtained applying the model on MRI acquisitions are presented for muscle and liver. For both tissues, the derived values of the water content and the dielectric properties at 128 MHz are reported first. Then the wideband dielectric behaviour obtained inserting these quantities in the model is shown in the frequency range 10 MHz–3 GHz. Results are compared with the open-probe measurements conducted in the same frequency band.

3.4.1. Water content derivation

The T_1 weighted image, derived with equation (17), is shown in figure (7) for the mixtures with a water content of 100% and 70% and for the two ex vivo tissues. The image was acquired in the transversal section of the central part of the beakers containing the materials.

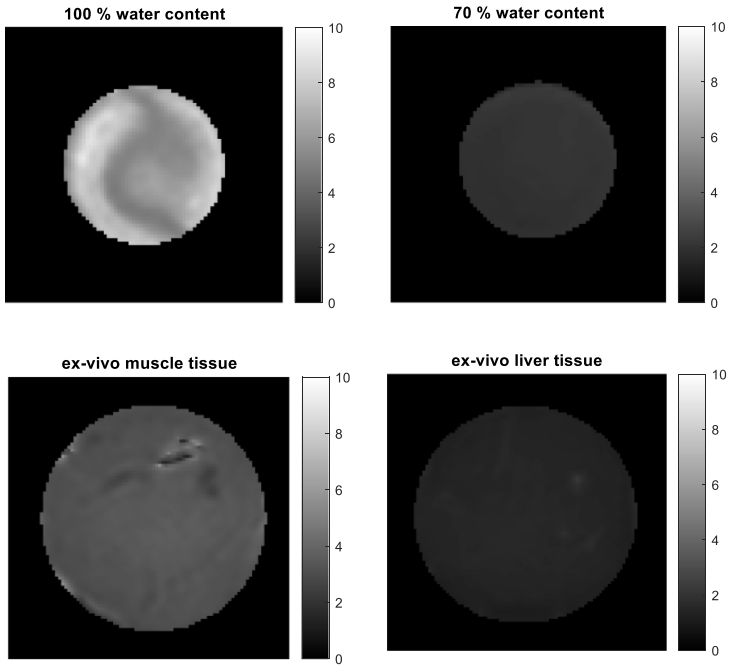

Figure 7. T_1 weighted image for the water-based mixtures and the ex vivo tissues.

Table 6. Average T_1 dependent signal in each beaker.

Material	Average signal intensity
100% water content mixture	5.74
70% water content mixture	2.70
Muscle tissue	3.27
Liver tissue	2.49

From the figure it is possible to observe that the brightness of the signal increases with the water content of the materials. For each beaker, the average value of the T_1 weighted map was computed in the whole section and is reported in table 6.

The values reported in the table for the water-based mixtures were used to calibrate the empirical formula (equation (16)) obtaining the coefficients A and B as 0.0062 and 0.0218, respectively. Using these coefficients in equation (16) and inserting the T_1 dependent data of muscle and liver (table 6), the water content of these tissues was determined. For muscle the average water content value was found to be 77.6% while for liver an average value of 66.8% was obtained. The variability of the derived quantity was computed as previously explained considering the mixtures with a known water content of 90% and 74%. The water content maps of these mixtures (figure (8)) were derived and then the average values were computed. For the 90% mixture an average water content of 91.84% was obtained with a variability of 1.84% from the ground truth. For the 74% mixture, the water content was found to be 71% with a variability of 3%. So, considering the worst-case scenario, the variability of 3% was taken into account. The final result of water content for muscle and liver was then 77.6% $\pm$ 3% and 66.8% $\pm$ 3%, respectively, in an agreement with literature data. In fact, the water content values reported in the literature for muscle and liver are in the range 72%–79% (Pethig and Kell 1987, Scheppes and Foster 1980, Mohammed *et al* 2020) and 65%–79% (Pethig and Kell 1987, Scheppes and Foster 1980, Mohammed *et al* 2020), respectively.

3.4.2. Forward EPT approach

Tables 7 and 8 show the real and the imaginary part of the permittivity of muscle and liver obtained at 128 MHz with the simplified forward Helmholtz method. As previously explained, the EPT data are obtained as the modal value in the dielectric properties' maps after applying denoising and segmentation procedures on the amplitude and phase of the transmit field. In the tables, the standard deviation both for the values higher and lower than the modal one is also shown. As a comparison, the results obtained with the open-ended probe measurements are reported as average values and corresponding uncertainty. In addition to that, values taken from the literature (Hasgall *et al* 2022) for the dielectric properties of muscle and liver at

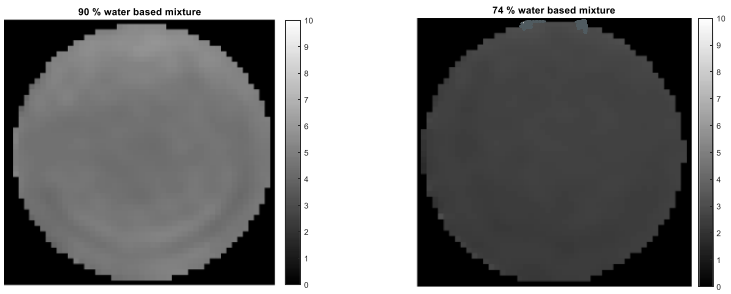

Figure 8. Water content map for the 90% and 74% mixtures.

Table 7. Real part of permittivity of tissues.

Tissue	$\varepsilon'_{\mathbf{R},128\ \mathbf{MHz}}$ (H-EPT)	$\varepsilon'_{\mathbf{R},128\ \mathbf{MHz}}$ (open probe)	$\varepsilon'_{\mathbf{R},128\ \mathbf{MHz}}$ (literature (Hasgall *et al* 2022))	$\Delta\varepsilon'_{\mathbf{R},\ 128\ \mathbf{MHz}}$ open probe/ H-EPT (%)	$\Delta\varepsilon'_{\mathbf{R},\ 128\ \mathbf{MHz}}$literature (Hasgall *et al* 2022)/ H-EPT (%)	$\Delta\varepsilon'_{\mathbf{R},\ 128\ \mathbf{MHz}}$literature (Hasgall *et al* 2022)/ open probe(%)
Muscle	[55.6−0.619; 55.6 + 14.4]	77.5 ± 3.56	63.5	28.2	12.4	18.1
Liver	[65.8−13.8; 65.8 + 9.37]	66.3 ± 3.00	64.3	8.60	2.33	3.11

Table 8. Imaginary part of permittivity of tissues.

Tissue	$\varepsilon''_{\mathbf{R},128\ \mathbf{MHz}}$ (H-EPT)	$\varepsilon''_{\mathbf{R},128\ \mathbf{MHz}}$ (open probe)	$\varepsilon''_{\mathbf{R},128\ \mathbf{MHz}}$(literature (Hasgall *et al* 2022))	$\Delta\varepsilon''_{\mathbf{R},\ 128\ \mathbf{MHz}}$ open probe/ H-EPT (%)	$\Delta\varepsilon''_{\mathbf{R},\ 128\ \mathbf{MHz}}$literature (Hasgall *et al* 2022)/ H-EPT (%)	$\Delta\varepsilon''_{\mathbf{R},\ 128\ \mathbf{MHz}}$ literature (Hasgall *et al* 2022)/ open probe(%)
Muscle	[134.1−72.43; 134.00 + 68.70]	95.54 ± 5.230	101.0	40.30	32.77	5.406
Liver	[90.80−46.28; 90.80 + 58.28]	70.95 ± 3.880	71.79	27.90	26.44	1.183

128 MHz are reported in the tables. The percentage error ($\Delta\varepsilon'^{(\prime\prime)}_{R,128\ \mathrm{MHz}}\%$) between the modal values obtained with EPT and the open probe ones, as well as percentage differences between literature values and the two experimental approaches, i.e. H-EPT and open-ended probe, were computed and are also reported in tables 7 and 8.

From the tables it is possible to notice that the results obtained with the EPT approach are characterised by a high standard deviation. This variability is due to the noise that affects the MRI signal and that is amplified by the second order derivative in the Helmholtz formulas (equations (24) and (25)). For the liver case a good agreement between the EPT data and the measurements with the open probe was obtained for the real part of permittivity with a corresponding percentage error of 8.6%. A higher error was obtained for the imaginary part of the same tissue, with a value of 27.9%. For muscle, a percentage error of 28.2% was found for the real part of the permittivity while an even higher error (40.3%) was obtained for the imaginary part. However, considering the high variability of the data it is possible to identify an agreement between the EPT results and the measurements obtained with the open probe. The comparison between EPT data and literature values show percentage errors slightly lower than the ones obtained from the comparison between EPT data and open probe measurements. For muscle a percentage error of 12.4% and 32.77% was obtained for the real and the imaginary part of permittivity, respectively, while for liver the values of 2.33% and 26.44% were obtained. Finally, the difference between the measurements obtained with the open probe and literature data is about 18% for the real part of permittivity of muscle and below 6% in all other cases. Given that the samples measured in (Hasgall *et al* 2022) are clearly different than the ones considered in this work, this difference highlights the need of a non-invasive technique for the dielectric characterization of specific samples.

3.4.3. Experimental validation of the model: wideband results

The derived values of water content and dielectric properties at 128 MHz were used in the dielectric model to reconstruct the real and the imaginary part of permittivity of ex vivo muscle and liver tissues in the frequency

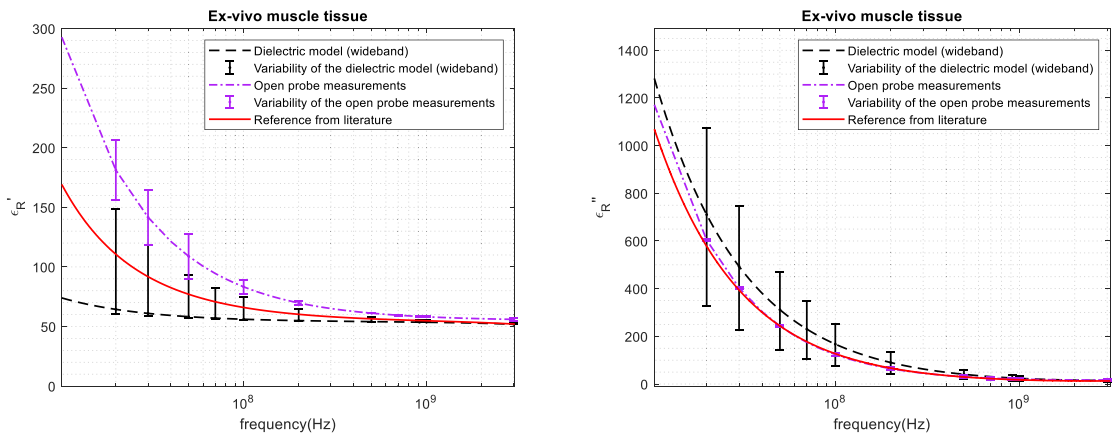

Figure 9. (a) Real and (b) imaginary part of the permittivity of muscle.

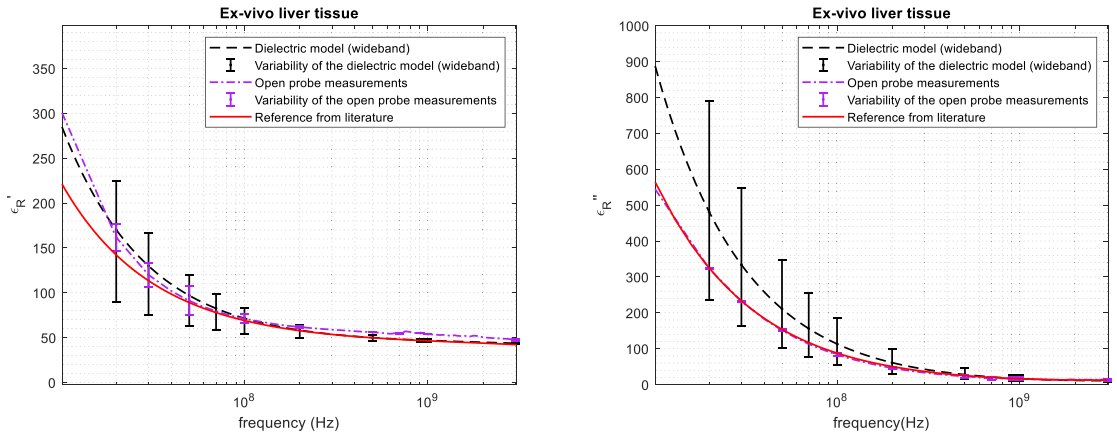

Figure 10. (a) Real and (b) imaginary part of the permittivity of liver.

range 10 MHz–3 GHz. This frequency interval was considered since it was the same of the measurements with the open probe technique.

Figures 9 and 10 show the dielectric properties of muscle and liver obtained using the model (dashed black curves) together with the measurements done with the open-ended probe technique (dashed—dotted violet curves) and the reference from literature (continuous red curves). The vertical lines represent the variability associated with the results. For the adopted model the variability was calculated considering the variability of the water content derivation and the one associated with the EPT data. For the open-ended probe measurements, the variability was given mainly by the measurement accuracy (equation (27)) since the one associated with the measurement repeatability (equation (29)) was negligible (<0.05%).

From the figures it is possible to notice that the variability of the EPT data affect the wideband results obtained with the dielectric model in a relevant way. Considering these variabilities, the dielectric properties reconstructed with the model comprehend those obtained with the open probe measurements and those taken from the literature. However, the results obtained from the modal value of the EPT data, i.e. without considering the variabilities, shown a different accuracy depending on the case. In the case of muscle (figure 9), data derived with the model are lower than the measured ones especially at low frequencies (<100 MHz) resulting in high percentage errors (higher than the 100% and equal to 26% for the real and imaginary part of permittivity, respectively). In the case of liver (figure 10), the values obtained with the proposed model show a better agreement with the open-ended probe measurements. A maximum percentage error of 14.8% and 63.9% is obtained for the real and the imaginary part of permittivity, respectively. As previously explained, the forward Helmholtz EPT approach, even if characterised by many

advantages, if affected by noise and boundary effects that have a negative impact on the results. Even in the literature it was shown that the reconstruction of the dielectric properties through EPT can show different variabilities depending on the adopted approach; using the forward Helmholtz approach, variabilities higher than 100% have been reported Mandija *et al* (2019). Additionally, the used approximations (equations (22) and (23)) could also affect the results. For this reason, when reconstructing the dielectric properties of a specific subject with this EPT method these drawbacks must be considered and, if possible, reduced.

4. Conclusions

This work presented a method for the evaluation of dielectric properties of biological tissues in a wide frequency band starting from quantities that can be acquired from MRI signals. It was shown that, knowing the water content and the dielectric properties at the MRI scanner frequency in the anatomical section of interest, it is possible to obtain the dielectric characterization of biological tissues specifically for each patient. This represents the main advantage of the adopted dielectric model since dielectric properties of human tissues are highly variable depending on the subject and health status. The theorical application of the model for muscle and fat using literature values showed a good agreement with the reference from literature in the whole considered frequency range (10 MHz–20 GHz). In particular, the maximum error was always lower than 10% for the real and the imaginary part of permittivity of muscle and for the real part of permittivity of fat. For the imaginary part of permittivity of this latter tissue, instead, the error reached about 17% at high frequencies (20 GHz). It is worth noticing here that the dielectric model was applied using water content values taken from the literature, considering works different from those taken into account for the dielectric properties' reference values. This difference in the source of the data introduces an uncertainty in the calculated values which is reflected into the reported errors. To evaluate the dependence of the model on uncertainties on the measurable quantities, a sensitivity analysis was conducted. It was proven that the presented approach can give quite accurate values of dielectric properties even when the input quantities are associated with a certain variability.

Finally, the model was applied experimentally using MRI acquisitions to reconstruct the dielectric properties of ex vivo muscle and liver tissues. The obtained results were compared with measurement performed by the open probe technique in the frequency range 10 MHz–3 GHz. The results show a good agreement especially for the case of liver while a greater difference was obtained for muscle. As shown in tables 7 and 8, the main source of error for muscle is the determination of the dielectric properties at the frequency of the scanner through the forward Helmholtz-based EPT approach. In this work the forward Helmholtz method was chosen for its simplicity and because, with respect to other methods, it relies on a physical basis. However, due to the presence of boundary errors and noise in the MRI images, it shows some limits. These can be overcome adopting different EPT approaches like the CSI-EPT or the deep learning techniques that can provide more accurate results but are more complex to implement.

It must be noted here that the EPT data used in the model were calculated at two different frequencies for the theoretical case (64 MHz) and the experimental one (128 MHz). This difference was due to an unexpected change in the availability of the MRI scanner. However, the good results achieved with both the theoretical and the experimental approaches show that the proposed model can be applied whichever scanner is used.

To conclude, the experimental study showed encouraging results and demonstrated the capability of the dielectric model to derive the dielectric behaviour of biological tissues starting from MRI acquisitions. Future steps of this work will consider the implementation of other EPT approaches, more accurate than the forward Helmholtz one adopted in this work, for the derivation of the low frequency term of the model. Additionally, the wideband model will be applied on different ex vivo tissues and on *in vivo* patients in order to prove its applicability in clinical procedures.

Data availability statement

All data that support the findings of this study are included within the article (and any supplementary information files).

Acknowledgments

The authors gratefully acknowledge the University Medical Centre of Amsterdam (UMC, Academic Medical Center AMC) for the possibility of using the 3 T MRI scanner, the expert support of J H Creeze and Z van Kesteren (UMC, Academic Medical Center AMC) and the advices provided by S Mandija (UMC, University Medical Center, Utrecht).

ORCID iDs

Flavia Liporace https://orcid.org/0000-0002-4490-1826
Marta Cavagnaro https://orcid.org/0000-0002-7624-1113

References

Andreuccetti D , Fossi R and Petrucci C 1997 An Internet resource for the calculation of the dielectric properties of body tissues in the frequency range 10 Hz - 100 GHz. IFAC-CNR. Based on data published by C.Gabriel *et al* in 1996 (available at: http://niremf.ifac.cnr.it/tissprop)

Bonkovsky H L 1991 Iron and the liver *Am. J. Med. Sci.* **301** 32–43

Cihoric N *et al* 2015 Hyperthermia-related clinical trials on cancer treatment within the ClinicalTrials.gov registry *Int. J. Hyperth.* **31** 609–14

Collins C M, Yang B, Yang Q X and Smith M B 2002 Numerical calculations of the static magnetic field in three-dimensional multi-tissue models of the human head *Magn. Reson. Imaging* **20** 413–24

Crooks L E 1985 An introduction to magnetic resonance imaging *IEEE Eng. Med. Biol. Mag.* **4** 8–15

Farace P, Pontalti R, Cristoforetti L, Antolini R and Scarpa M 1997 An automated method for mapping human tissue permittivities by MRI in hyperthermia treatment planning *Phys. Med. Biol.* **42** 2159–74

Fatouros P P and Marmarou A 1999 Use of magnetic resonance imaging for in vivo measurements of water content in human brain: method and normal values *J. Neurosurg.* **90** 109–15

Fricke H 1924 A mathematical treatment of the electric conductivity and capacity of disperse systems I. The electric conductivity of a suspension of homogeneous spheroids *Phys. Rev.* **24** 575–87

Gabriel C, Gabriel S and Corthout E 1996 The dielectric properties of biological tissues: i. Literature survey *Phys. Med. Biol.* **41** 2231–49

Gabriel S, Lau R W and Gabriel C 1996a The dielectric properties of biological tissues: II. Measurements in the frequency range 10 Hz-20 GHz *Phys. Med. Biol.* **41** 2251–69

Gabriel S, Lau R W and Gabriel C 1996b The dielectric properties of biological tissues: III. Parametric models for the dielectric spectrum of tissues *Phys. Med. Biol.* **41** 2271–93

Godinho D M, Felício J M, Castela T, Silva N A, Orvalho M L, Fernandes C A and Conceição R C 2021 Development of MRI-based axillary numerical models and estimation of axillary lymph node dielectric properties for microwave imaging *Med. Phys.* **48** 5974–90

Gregory A P and Clarke R N 2007 Dielectric metrology with coaxial sensors *Meas. Sci. Technol.* **18** 1372

Grover V P, Tognarelli J M, Crossey M M, Cox I J, Taylor-Robinson S D and McPhail M J 2015 Magnetic resonance imaging: principles and techniques: lessons for clinicians *J. Clin. Exp. Hepatol.* **5** 246–55

Hasgall P A , Di Gennaro F , Baumgartner C , Neufeld E , Lloyd B , Gosselin M C , Payne D , Klingenbock A and Kuster N 2022 IT'IS Database for thermal and electromagnetic parameters of biological tissues, Version 4.1 (https://doi.org/10.13099/VIP21000-04-1)

Hoult D I 2000 The principle of reciprocity in signal strength calculations—a mathematical guide *Concepts Magn. Res.* **12** 173–87

Kaatze U 2011 Bound water: evidence from and implications for the dielectric properties of aqueous solutions *J. Mol. Liq.* **162** 105–12

Katscher U and van den Berg C A T 2017 Electric properties tomography: biochemical, physical and technical background, evaluation and clinical applications *NMR Biomed.* **30** e3729

Katscher U, Voigt T, Findeklee C, Vernickel P, Nehrke K and Dössel O 2009 Determination of electric conductivity and local SAR via B1 mapping *IEEE Trans. Med. Imaging* **28** 1365–74

Leijsen R, Brink W, van den Berg C, Webb A and Remis R 2021 Electrical properties tomography: a methodological review *Diagnostics* **11** 176

Liporace F and Cavagnaro M 2022 Use of the open-ended probe technique for the dielectric characterization of biological tissues at low frequencies *2022 Int. Workshop on Impedance Spectroscopy (IWIS)* (*Chemnitz, Germany*) pp 66–69

Liporace F and Cavagnaro M 2023 Development of MR-based procedures for the implementation of patient-specific dielectric models for clinical use *J. Mech. Med. Biol.* **23** 06

Liu J, Wang Y, Katscher U and He B 2017 Electrical properties tomography based on B1 maps in MRI: principles, applications, and challenges *IEEE Trans. Biomed. Eng.* **64** 2515–30

Malik N A, Sant P, Ajmal T and Ur Rehman M 2021 Implantable antennas for bio-medical applications *IEEE J. Electromagn. RF Microw. Med. Biol.* **5** 84–96

Mandija S, Meliadò E F, Huttinga N R F, Luijten P R and van den Berg C A T 2019 Opening a new window on MR-based electrical properties tomography with deep learning *Sci. Rep.* **9** 8895

Marsland T P and Evans S 1987 Dielectric measurements with an open-ended coaxial probe *IEE Proc.* H (Microwaves, Antennas and Propagation) **134** 341–49

Martinsen O G and Heiskanen A 2023 *Bioimpedance and Bioelectricity Basics* 4th edn (Elsevier) (https://doi.org/10.1016/C2018-0-04808-2)

Mattsson M-O and Simkò M 2019 Emerging medical applications based on non-ionizing electromagnetic fields from 0 Hz to 10 THz *Med. Devices* **12** 347–68

Mazzurana M, Sandrini L, Vaccari A, Malacarne C, Cristoforetti L and Pontalti R 2003 A semi-automatic method for developing an anthropomorphic numerical model of dielectric anatomy by MRI *Phys. Med. Biol.* **48** 3157–70

Michel E, Hernandez D and Lee S Y 2017 Electrical conductivity and permittivity maps of brain tissues derived from water content based on T_1 -weighted acquisition *Magn. Reson. Med.* **77** 1094–103

Mohammed B J, Manoufali M, Naqvi S A R, Bialkowski K S, Mills P C and Abbosh A M 2020 Using dielectric properties of solid fraction and water content to characterize tissues at different health and age conditions *IEEE J. Electromagn. RF Microw. Med. Biol.* **4** 69–77

Mosig J R, Besson J-C E, Gex-Fabry M and Gardiol F E 1981 Reflection of an open-ended coaxial line and application to non-destructive measurement of materials *IEEE Trans. Instrum. Meas.* **IM-30** 46–51

Pelicano A C, Gonçalves M C T, Godinho D M, Castela T, Orvalho M L, Araújo N A M, Porter E and Conceição R C 2021 Development of 3D MRI-based anatomically realistic models of breast tissues and tumours for microwave imaging diagnosis *Sensors* **21** 8265

Pethig R and Kell D B 1987 The passive electrical properties of biological systems: their significance in physiology, biophysics and biotechnology *Phys. Med. Biol.* **32** 933–70

Peyman A, Gabriel C and Grant E H 2007 Complex permittivity of sodium chloride solutions at microwave frequencies *Bioelectromagnetics* **28** 267–74

Peyman A, Kos B, Djokić M, Trotovšek B, Limbaeck-Stokin C, Serša G and Miklavčič D 2015 Variation in dielectric properties due to pathological changes in human liver *Bio Electromagn.* **36** 603–12

Sadleir R and Minhas A 2022 *Electrical Properties of Tissues: Quantitative Magnetic Resonance Mapping* vol 1380 (*Advances in Experimental Medicine and Biology*) (Springer) (https://doi.org/10.1007/978-3-031-03873-0)

Schabel M C and Parker D L 2008 Uncertainty and bias in contrast concentration measurements using spoiled gradient echo pulse sequences *Phys. Med. Biol.* **53** 2345–72

Schepps J L and Foster K R 1980 The UHF and microwave dielectric properties of normal and tumour tissues: variation in dielectric properties with tissue water content *Phys. Med. Biol.* **25** 1149–59

Sebek J, Albin N, Bortel R, Natarajan B and Prakash P 2016 Sensitivity of microwave ablation models to tissue biophysical properties: a first step toward probabilistic modelling and treatment planning *Med. Phys.* **43** 2649

Stuchly M A, Athey T W, Samaras G M and Taylor G E 1982 Measurement of radio frequency permittivity of biological tissues with an open-ended coaxial line: part II—experimental results *IEEE Trans. Microw. Theory Tech.* **30** 87–92

Stuchly M A and Stuchly S S 1980 Coaxial line reflection methods for measuring dielectric properties of biological substances at radio and microwave frequencies-a review *IEEE Trans. Instrum. Meas.* **29** 176–83

Taylor B N and Kuyatt C E 1994 Guidelines for evaluating and expressing the uncertainty of NIST measurement results *NIST Technical Note,* 1297 1994 edn

Tuncer E, Serdyuk Y V and Gubanski S M 2002 Dielectric mixtures: electrical properties and modeling *IEEE Trans. Dielectr. Electr. Insul.* **9** 809–28

van Lier A L, Raaijmakers A, Voigt T, Lagendijk J J, Luijten P R, Katscher U and van den Berg C A 2014 Electrical properties tomography in the human brain at 1.5, 3, and 7T: a comparison study *Magn. Reson. Med.* **71** 354–63

Voigt T, Nehrke K, Doessel O and Katscher U 2010 T1 corrected B1 mapping using multi-TR gradient echo sequences *Magn. Reson. Med.* **64** 725–33

Yarnykh V L 2007 Actual flip-angle imaging in the pulsed steady state: a method for rapid three-dimensional mapping of the transmitted radiofrequency field *Magn. Reson. Med.* **57** 192–200